PAPER

Simple Primary User Signal Area Estimation for Spectrum Measurement

Kenta UMEBAYASHI[†a)], **Kazuki MORIWAKI**[†], ***Members***, **Riki MIZUCHI**[†], ***Nonmember***, **Hiroki IWATA**[†], ***Student Member***, **Samuli TIIRO**[†], ***Nonmember***, **Janne J. LEHTOMÄKI**[††], ***Member***, **Miguel LÓPEZ-BENÍTEZ**[†††], ***Nonmember***, ***and*** **Yasuo SUZUKI**[†], ***Fellow***

SUMMARY This paper investigates a signal area (SA) estimation method for wideband and long time duration spectrum measurements for dynamic spectrum access. SA denotes the area (in time/frequency domain) occupied by the primary user's signal. The traditional approach, which utilizes only Fourier transform (FT) and energy detector (ED) for SA estimation, can achieve low complexity, but its estimation performance is not very high. Against this issue, we apply post-processing to improve the performance of the FT-based ED. Our proposed method, simple SA (S-SA) estimation, exploits the correlation of the spectrum states among the neighboring tiles and the fact that SA typically has a rectangular shape to estimate SA with high accuracy and relatively low complexity compared to a conventional method, contour tracing SA (CT-SA) estimation. Numerical results will show that the S-SA estimation method can achieve better detection performance. The SA estimation and processing can reduce the number of bits needed to store/transmit the observed information compared to the FT-based ED. Thus, in addition to improved detection performance it also compresses the data.

key words: *dynamic spectrum access, smart spectrum access, spectrum measurement, cognitive radio, signal detection, signal area estimation*

1. Introduction

In the wireless communication field, spectrum scarcity problem is a pressing problem. On the other hand, spectrum utilization measurement reports have revealed that the utilization rate of most of the licensed spectrum is not very high in spatial and/or temporal domains. The portions of spectrum left unused are commonly referred to as white space (WS) [1]. For this problem, dynamic spectrum access (DSA) with cognitive radio [2] techniques employed by the unlicensed user (secondary user: SU) on the spectrum owned by the licensed user (primary user: PU) have been investigated [3], [4]. In the DSA, the SU can utilize the vacant spectrum as long as it will not cause any harmful interference to the PU. To enable DSA, a technique for understanding the state of the spectrum, i.e. whether it is vacant or occupied, is necessary.

Spectrum sensing [5] and geolocation database [6] techniques have been investigated in order to resolve the spectrum state. The database based techniques are suitable for static broadcast systems such as TV but spectrum sensing is rather more appropriate for wireless systems with dynamic PU traffic since it attempts to recognize the instantaneous state of the spectrum. In addition, the DSA system does not need to rely on an external system to obtain state information of the spectrum. This is another advantage of spectrum sensing. However, spectrum sensing typically requires high accuracy, low latency and low cost which are very difficult to achieve [5]. One potential approach to solving the issue in spectrum sensing is smart spectrum access (SSA) which is an extended DSA that utilizes useful prior information, such as statistical information in terms of PU spectrum utilization [7]. It has been shown that using statistical information can enhance the spectrum sensing performance [8], [9]. In addition, it can enhance other techniques employing vacant spectrum utilization, such as spectrum management, channel selection and MAC protocol design [10]–[13].

One important issue in SSA is the implementation cost of the function obtaining the prior information, especially at wireless terminals. For this issue, we proposed a system architecture consisting of two layers in [7]: the first layer corresponds to a DSA system and the second layer is a spectrum awareness system (SAS). Concept of the two layer SSA is shown diagrammatically in Fig. 1. In the two-layer SSA, the SAS is dedicated for spectrum measurement to obtain the prior information. Therefore, DSA terminals

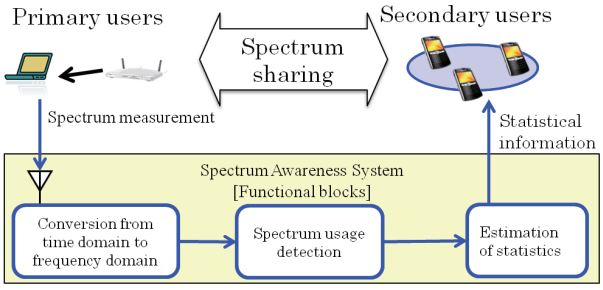

Fig. 1 Concept of Two layered Smart Spectrum Access (SSA). First layer: DSA. Second Layer: Spectrum Awareness System (SAS).

Manuscript received June 7, 2015.
Manuscript revised October 4, 2015.

[†]The authors are with the Graduate School of Engineering, Tokyo University of Agriculture and Technology, Koganei-shi, 184-8588 Japan.

[††]The author is with the Centre for Wireless Communications, University of Oulu, P. O. BOX 4500 FIN-90014 University of Oulu, Finland.

[†††]The author is with the Department of Electrical Engineering and Electronics, University of Liverpool, Merseyside, L69 3GJ, United Kingdom.

a) E-mail: ume_k@cc.tuat.ac.jp

DOI: 10.1587/transcom.2015EBP3240

no longer suffer from the high implementation cost, but the useful information is provided by the SAS. The SAS consists of three functional blocks, time-frequency domain conversion (such as FFT: fast Fourier transform) which obtains the power spectrum density (PSD), spectrum usage detection, and extraction of prior information based on analysis of the spectrum usage detection results. In this paper, we focus on the second functional block, spectrum usage detection. Since this process is performed continuously to recognize spectrum usage patterns, output of the signal usage detection is in the form of a two-dimensional time/frequency grid. Let us denote a single element of the grid corresponding to one time slot and one frequency bin by tile. A rectangular set of contiguous tiles wherein a PU signal is detected is referred to as estimated signal area (SA). The ultimate objective of this work is to identify and estimate SAs within the aforementioned time/frequency grid in an accurate and efficient manner.

In the SAS, multiple observation equipments (OEs) are deployed to cover a broad area. The role of the OE is to observe the spectrum and send the observed information, i.e. tiles detected as vacant or occupied, to a central control station such as a fusion center (FC). In this case, requirements of the OE are as follows; accurate detection performance, relatively low computational cost and low amount of information in terms local observed information. However, latency requirements in spectrum measurement are relaxed compared to spectrum sensing.

There are several spectrum measurement campaigns for the assessment of WS based on spectrum usage detection [6], [14]–[16]. In most of the spectrum measurements, FFT-based energy detector (ED) is used to detect PU spectrum utilization in the considered frequency bins. This approach is denoted by Fourier transform based ED (FT-ED) in this paper.

Output of the FT-ED based spectrum measurement consists of signal detection results in tiles. Detection result $\hat{H}$ can be either H_1 (the tile is occupied by PU signal) or H_0 (the tile is not occupied). In signal detection, there are two errors: the first one is missed detection ($\hat{H} = H_0|H_1$) where $|$ means given that correct hypothesis is H_1, and the second one is false alarm ($\hat{H} = H_1|H_0$).

ED is very simple and does not require any prior information about the PU signal [17], however the detection performance is not very high. On the other hand, the other methods such as feature detection and cyclostationary detection can achieve better detection performance but they require prior information about PU signal and high computational cost [5].

One possible approach to improve the detection performance of FT-ED is to utilize neighboring detection results in an SA. Now we define SA as follows: a cluster of $\hat{H} = H_1$ tiles due to one continuous signal transmission such as one data packet. The time duration of SA is determined by the time duration of the continuous signal and the bandwidth of the SA is determined by the symbol rate and band limited filter used in the transmitter. SA has typically a rectangular shape [18], since symbol rate is typically fixed during one continuous signal.

There are several methods employing the above approach, such as in the localization algorithm based on double-thresholding (LAD) method with adjacent cluster combining (ACC) [19] and improved energy detection [20]. In [21], FT-ED is used and clusters of connected $\hat{H} = H_1$ tiles are obtained by using standard contour tracing (CT) techniques [22]. The estimated SAs are the smallest rectangles that cover each cluster. We call the approach used in [21] as CT-SA and use it as a baseline for comparisons with our proposed method. Improvement of detection performance in the above approaches is achieved by time and frequency diversity gains.

In this paper, we propose an SA estimation based on the output of the Welch FFT based ED by considering the requirements of OE. Welch FFT [23] based ED is one of FT-ED approaches and it can achieve better detection performance compared to typical FFT based ED [24]. Our main contributions in this paper are summarized as follows:

- Simple-SA (S-SA) estimation is proposed in this paper. Unlike conventional CT-SA estimation, S-SA estimates the width corresponding to frequency domain and the height corresponding to time domain of the rectangle which leads to less complexity. Similar to CT-SA, S-SA combines the several detection results in time and frequency domains and it can recognize SA accurately.
- SA estimation approaches including S-SA and CT-SA estimations can inherently increase the detection probability but also the false alarm probability. For this problem, we propose a False alarm Cancellation (FC) method to further improve the detection performance.
- In SA estimation approaches, the estimated SA always has a rectangular shape. We propose a data compression method that exploits this feature by expressing the observed information by the rectangles instead of outputs of FT-ED.
- Extensive performance evaluations are performed verifying the performances and complexity benefits of S-SA estimation compared with the FT-ED and CT-SA. We also confirm the reduction of the amount of information regarding the spectrum measurement by numerical evaluation.

The remainder of this paper is organized as follows: generic outline of signal processing in OE is provided in Sect. 2. The SA estimation methods, CT-SA estimation and S-SA estimation, are described in Sect. 3. The FC method which can enhance S-SA estimation is also shown in Sect. 3. A design criterion of S-SA is shown in Sect. 4. In Sect. 5, numerical results will show the advantages of S-SA estimation. The conclusions are drawn in Sect. 6.

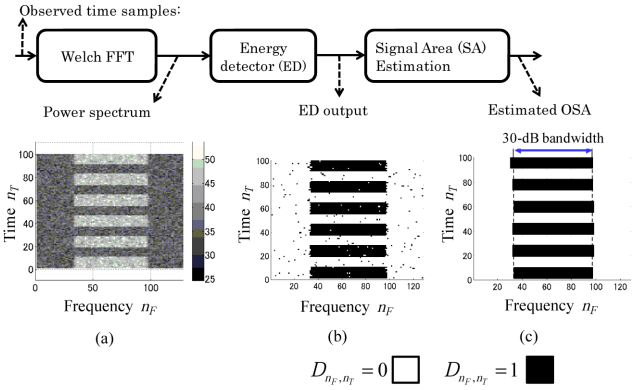

Fig. 2 Block diagram for spectrum measurement in OE.

2. Outline of Signal Processing in Observation Equipment (OE)

A block diagram of the signal processing flow in OE is shown in Fig. 2. the role of OE is to observe spectrum usage of the PU. The signal processing in the OE consists of three processes; Welch FFT, ED, and SA estimation. The details about ED based on Welch FFT are provided in our earlier paper [24].

Observed samples are obtained at f_S Hz sampling rate. The center frequency of the observed spectrum is set to 0 Hz by downconversion, and it is band-limited to $[-f_S/2, f_S/2]$ Hz.

To obtain PSD, Welch FFT is used and the number of samples in time domain for single Welch FFT is denoted by N_S. The N_S samples resulting from the Welch FFT correspond to a single time slot. We also set the number of time slots in one observation to N_{timeslot}. Therefore, the time duration for one observation is given by $(N_{\text{timeslot}} \times N_S)/f_S$ sec.

In the Welch FFT, N_S samples are divided into N_{seg} segments where the number of samples in one segment is denoted by N_W. In a typical FFT, N_S is set to a power of two. Without loss of generality, N_W is also assumed to be a power of two[†] and N_{seg} is given by

$$N_{seg} = \frac{N_S - N_W}{N_O} + 1 = \frac{2N_S}{N_W} - 1, \tag{1}$$

where N_O indicates overlapped samples which is set to $N_O = N_W/2$ and $N_S > N_W$. The obtained PSD values are denoted by P_{n_F,n_T} where $n_F \in \{1, 2, ..., N_{\text{W}}\}$ and $n_T \in \{1, 2, N_{\text{timeslot}}\}$ are the frequency and time index numbers of the tile. The Fig. 2(a) shows an example of the PSD values. In the Welch FFT, Hamming window is used.

The ED provides signal detection result at the tile (n_F, n_T) and it is given by

$$D^{(\text{ED})}_{n_F,n_T} = \begin{cases} 1 & (P_{n_F,n_T} > \tau) \\ 0 & (\text{otherwise}), \end{cases} \tag{2}$$

[†] N_{seg} is the number of samples in a segment, which must be an integer number. Given (1), this requires N_W to be an integer divisor of N_S. Since N_S is a power of two, all divisors of N_S are powers of two and N_W also needs to be a power of two for this to be true.

where $D^{(\cdot)}_{n_F,n_T} = 1$ and $D^{(\cdot)}_{n_F,n_T} = 0$ indicate that the tile at (n_F, n_T) is either estimated to be occupied by PU signal or vacant, respectively, the superscript notation $(\cdot)$ indicates the method to obtain the decision such as ED and S-SA estimation, and τ is the threshold for ED. Fig. 2(b) shows an example of $D^{(\text{ED})}_{n_F,n_T}$.

There are several ways to define the bins where signal is actually present. We use the 30-dB bandwidth [25], so that the signal bandwidth is defined by the frequency bins when the signal power is 30 dB below its peak value. The corresponding SA is defined by the signal bandwidth and the time duration of the continuous signal emission. A correct decision for a frequency bin within this area is H_1 otherwise H_0 is correct.

We define false alarm probability for the output of ED as $\text{P}_{\text{FA}}{}^{(\text{ED})} = \Pr(D^{(\text{ED})}_{n_F,n_T} = 1 | H(n_F, n_T) = H_0)$ where $H(n_F, n_T)$ indicate the spectrum state in the tile at (n_F, n_T) and H_0 indicates that the tile is not occupied by PU signal. In addition, detection probability ($\text{P}_{\text{D}}{}^{(\text{ED})}$) indicates that $\text{P}_{\text{D}}{}^{(\text{ED})} = \Pr(D^{(\text{ED})}_{n_F,n_T} = 1 | H(n_F, n_T) = H_1)$ where H_1 indicates that the tile is occupied by PU signal.

All the SA estimation approaches utilize the outputs from ED and process them. Due to processing, the false alarm probability in the output may change compared to the false alarm probability in the input data. Thus in SA estimation, there are two false alarm probabilities, such as $\text{P}_{\text{FA}}{}^{(\text{ED})}$ and $\text{P}_{\text{FA}}{}^{(\text{S-SA})}$ (or $\text{P}_{\text{FA}}{}^{(\text{CT-SA})}$). We employ constant false alarm rate (CFAR) criterion and threshold τ is set based on target false alarm rate $\tilde{\text{P}}^{(\text{S-SA})}_{\text{FA}}$, where $\tilde{}$ indicates target value.

The description of general behavior of SA estimation shown in (b) and (c) of Fig. 2 is described as follows. In Fig. 2(b), $D^{(\text{ED})}_{n_F,n_T}$ (ED output) are clusters colored by dark color and they are almost rectangular. The SA estimation recognizes the clusters and approximates them to rectangles as shown in Fig. 2(c). The white colored tiles ($D^{(\text{ED})}_{n_F,n_T} = 0$) inside the rectangles in Fig. 2(b) are missed detections. The SA estimation has a potential to reduce the missed detections by filling the white colored tiles within rectangle.

3. Signal Area Estimation

The general outline of the process common to both CT-SA and S-SA estimation methods is illustrated in Fig. 3. In both SA estimation methods, the first step of the algorithm is to find a starting point for the occupied signal area. This is done by performing a raster scan on the spectrum grid from left to right and bottom to up until the first occupied tile, i.e. $D^{(\text{ED})}_{n_F,n_T} = 1$, is found. The coordinates of the first tile are denoted by $\mathbf{S}$ and in the example of Fig. 3(a) are equal to $\mathbf{S} = (3, 2)$. After this, each method estimates the occupied signal area, and provides an estimation result as a rectangle which covers the area as shown in Fig. 3-(b). The output of the estimation is denoted by estimated rectangle SA in this paper. In the SA approach, the estimation result can be represented with a corner coordinate, and the width and height of the rectangle, such as A, $\hat{W}$, and $\hat{H}$ in Fig. 3-(b). However, the spectrum grid obtained with an ED represents sig-

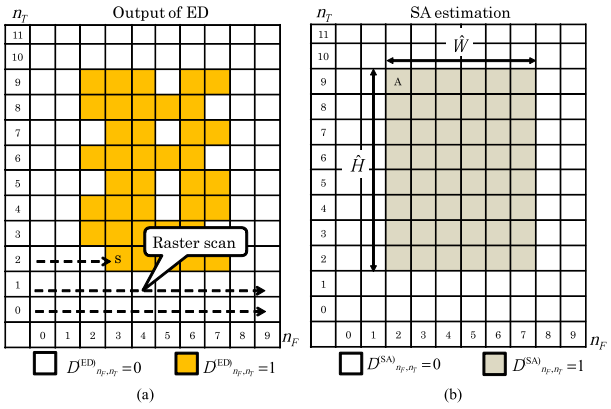

Fig. 3 Example outputs of ED and SA estimation.

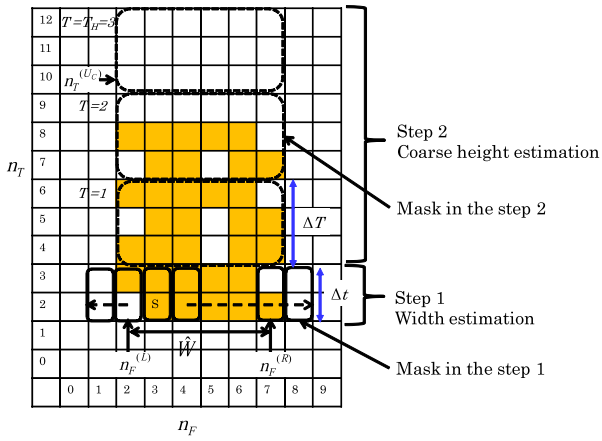

Fig. 4 Process of S-SA step 1 and step 2.

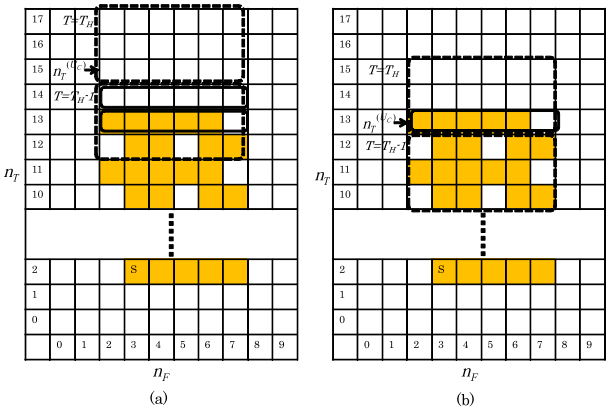

Fig. 5 Process of S-SA step 3.

nal occupancy information in the observed time-frequency space. Therefore, in wideband or long-term measurements rectangular signal area estimate has the benefit of reducing the amount of required information. This will be confirmed in Sect. 5.

In our implementation of the CT-SA [21], we used the standard CT technique [22] which can obtain the cluster of connected tiles with $D^{(\mathrm{ED})}_{n_F,n_T} = 1$. The estimated rectangle SA corresponds to the minimum rectangle which can cover the cluster.

Details of the successive process after the raster scan in the S-SA estimation are described in the following subsection.

The difference to the CT-SA method is that since S-SA is designed to estimate directly a rectangular area, on the other hand CT technique is designed to find arbitrary shape. Therefore, S-SA is generally simpler. Furthermore, since the estimation is performed using larger detection masks covering multiple tiles, it has the benefit of combining multiple masks and covering small gaps between tiles. With proper mask size, it is possible to improve SA estimation performance due to diversity gain by combining multiple ED decisions.

3.1 Simple SA Estimation

After finding the starting point **S**, the S-SA method consists of three separate steps: width estimation (step 1), coarse height estimation (step 2) and fine height estimation (step 3).

The first step of the S-SA method is the width estimation and the process is shown in Fig. 4. We set a parameter Δt which determines size of the detection mask used to detect signal area in the first step. Starting from $\mathbf{S} = (x_s, y_s)$ the algorithm checks the detected occupancy of tiles in $n_F = x_s$ and $y_s \le n_T \le y_s + \Delta t$. If one or more of these tiles are determined as occupied, the algorithm moves to the right to $n_F = x_s + 1$ and repeats the process. The right edge is found when all the tiles inspected are detected as unoccupied. The left edge can be found correspondingly by moving to the opposite direction from the starting point **S**. The left and right edge estimates are found as $n_F^{(L)}$ and $n_F^{(R)}$, respectively, which then provides the width estimate as $\hat{W} = n_F^{(R)} - n_F^{(L)} + 1$. In the example of Fig. 4, $n_F^{(L)} = 2$, $n_F^{(R)} = 7$ and $\hat{W} = 6$.

Next step provides a rough estimate for the height of the rectangle and an example can also be found in Fig. 4. Parameter ΔT is set which denotes the height of the detection mask and the width of the mask is set to $\hat{W}$. Threshold controlling the sensitivity is set to $0 < \gamma_{\mathrm{step2}} < 1$. The detection mask begins with its bottom row at time slot $x_s + \Delta t + 1$. The algorithm then checks the occupancy of the tiles covered by the mask are occupied and if more than $\gamma_{\mathrm{step2}} \times \hat{W}\Delta T$ tiles are detected as occupied, the area covered by the mask is determined as SA. This condition is denoted by sensitivity condition. The mask is then moved up by ΔT time slots and the process is repeated until a mask not satisfying the sensitivity condition is found. The index number of mask is denoted by T and $T = T_H$ at the first mask not satisfying the sensitivity condition. This then provides the rough estimate for the upper part of the estimated area as $n_T^{(U_C)}$ which corresponds to the bottom time slot in the T_Hth mask.

In the rough height estimation there are two different scenarios to consider which are illustrated in Fig. 5(a) and (b). In the scenario (a), the algorithm stops because there

are no occupied tiles in the last mask. On the other hand, in the scenario (b), the algorithm stops because of the sensitivity condition is not satisfied but there are still less than $\gamma_{\text{step2}} \times \hat{W}\Delta T$ occupied tiles in the mask above the estimated $n_T^{(U_C)}$ time slot. Therefore, a final height estimation step is performed to obtain a more accurate result. In this fine height estimation, the detection mask is set to $\hat{W}$ frequency bins and this corresponds to setting $\Delta T = 1$ in step 2. We also set a sensitivity parameter $0 < \gamma_{\text{step3}} < 1$ and check if more than $\gamma_{\text{step3}} \times \hat{W}$ tiles under the mask are occupied or not. The search starts at $n_T^{(U_C)}$. If the sensitivity condition is not satisfied at the $n_T^{(U_C)}$ time slot, it goes downwards to find a detection mask which satisfies the sensitivity condition. This corresponds to scenario (a) in Fig. 5 and the time slot satisfying the sensitivity condition is the final estimate $n_T^{(U_F)}$.

On the other hand, if the sensitivity condition is satisfied at the $n_T^{(U_C)}$ time slot, it goes to upwards to find a detection mask which does not satisfy the sensitivity condition. This corresponds to scenario (b) in Fig. 5 and the previous time slot of the time slot not satisfying the sensitivity condition is the final estimate $n_T^{(U_F)}$. The decision result obtained by S-SA is denoted by $D_{n_F,n_T}^{(\text{S-SA})}$ and the state of tiles inside the estimated SA is $D_{n_F,n_T}^{(\text{S-SA})} = 1$.

3.2 False Alarm Cancellation (FC)

The S-SA estimation can reduce missed detections, however it conversely increases the false alarm probability. In Fig. 6, two cases which may increase false alarms are shown.

In the case 1, false alarms (FA1 and FA2 in the figure) are adjacent and the S-SA causes overestimation by combining the tiles near the false alarms. In this case, state of tiles in $(n_F, n_T) = (1, 1)$ and $(n_F, n_T) = (0, 2)$ will be changed to 1 by the S-SA.

In the second case, a false alarm (denoted by FA3 in the figure) lies just below the actual SA. The S-SA estimation may overestimate the area where $4 \le n_F \le 9$ and $0 \le n_T \le 1$ due to the step 2 of S-SA estimation. This overestimation can occur if the distance between them is less than Δt. In fact, the increment of false alarms due to the SA estimation with the second case is the dominant.

For this issue, we propose a FC method which is a countermeasure for both cases. In image processing, several methods, such as mathematical morphology [26], have been investigated which can be applied to suppress false alarms. However, we propose a FC method for the S-SA estimation which is designed to combat the two aforementioned cases.

The FC is incorporated in the S-SA estimation and the block diagram is shown in Fig. 7. The FC method is implemented between step 1 and step 2 and it consists of two conditions. Specifically, if one of two conditions is not satisfied, it will determine that the state at **S** is a false alarm and change the state as $D_{x_s,y_s}^{(\text{ED})} = 0$.

The first condition is as follows: if $\hat{W} < 3$, the observed signal at S is determined the observed signal at **S** as

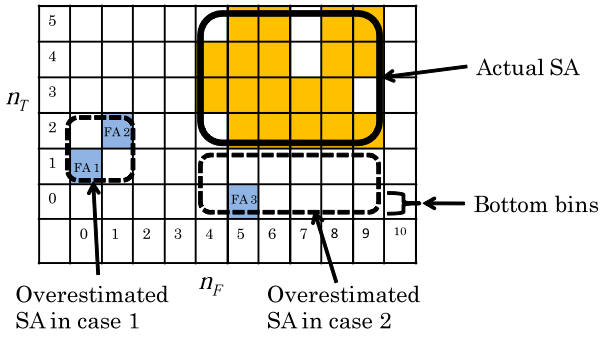

Fig. 6 Effect of false alarms (case 1 and case 2).

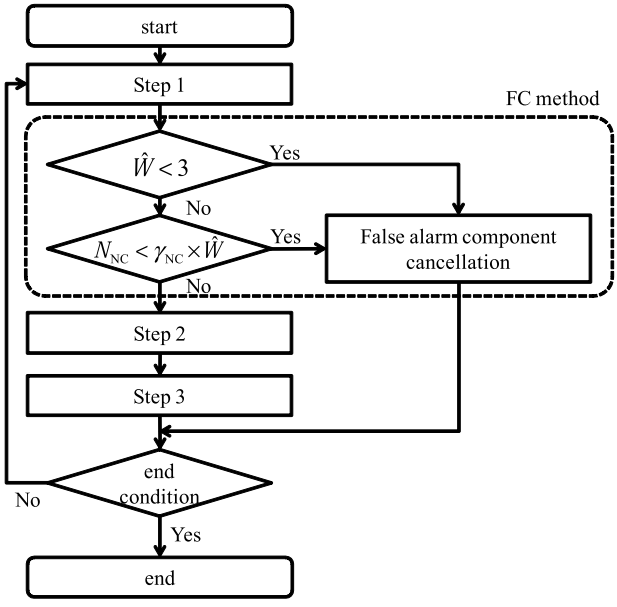

Fig. 7 Flow chart of S-SA with NF.

a false alarm component. The reason of the threshold set to three in the first condition is as follows. A correlation between neighboring frequency bins is not negligible due to the Hamming window used in the Welch FFT [27]. Since instantaneous false alarms in neighboring frequency bins are highly possible, we set the threshold to three. In the case 1 in Fig. 6, this condition can cancel the false alarms in FA1 and FA2.

In the second condition, the number of $D_{n_F,n_T}^{(\text{ED})} = 1$ tiles is counted at the bottom bins of the estimated SA in the step 1. In the example of Fig. 6, tiles at $4 \le n_F \le 9$ and $n_T = 0$ correspond to the bottom bins. The counted number is denoted by N_{FC} and the second condition is as follows: if $N_{\text{FC}} < \hat{W} \times \gamma_{\text{FC}}$, where γ_{FC} is a sensitivity parameter to control the threshold ($\hat{W} \times \gamma_{\text{FC}}$) and $0 < \gamma_{\text{FC}} < 1$, the observed signal at **S** is determined as a false alarm.

Through steps 1 - 3, a rectangle corresponding to the estimated signal area is obtained. An end condition of the SA estimation with FC shown in Fig. 7 occurs when the prearranged observed area is processed.

The decision result obtained by S-SA estimation with

FC is denoted by $D_{n_F,n_T}^{(\mathrm{S-SA-FC})}$ and only the inside of estimated rectangle is $D_{n_F,n_T}^{(\mathrm{S-SA-FC})} = 1$.

4. Design of S-SA

In the S-SA, there are four design parameters Δt, ΔT, γ_{step2}, and γ_{step3}. In this section, a possible design criterion is provided.

In fact Δt and ΔT are related to time resolution of spectrum usage measurement and this is one of the important parameters. Criterion for setting Δt and ΔT is based on the time resolution required to recognize spectrum usage pattern in the time domain correctly [16]. For thresholds γ_{step2}, and γ_{step3}, estimation accuracy, i.e. root mean square error (RMSE) in terms of width and height estimations, can be appropriate criterion.

Let $H_{\min}$ and $G_{H,\min}$ denote the minimum possible time duration of one continuous signal, such as one data packet, and the time gap between a string of two continuous signals, respectively. In the case of 2.4 GHz industry science medical (ISM) band, there are several types of wireless systems, such as IEEE 802.11 wireless local area network (WLAN). In the case of IEEE 802.11 WLAN, the time gap is given by for example time duration of distributed coordination function interframe space (DIFS). In fact, the applicability of this design is not limited to WLAN but it is applicable for other wireless systems.

Given $H_{\min}$ and $G_{H,\min}$, we set Δt as follows

$$\Delta t = \min[H_{\min}, G_{H,\min}] \tag{3}$$

On the other hand, ΔT can be set as

$$\Delta T = \min[H_{\min}, G_{H,\min}/2], \tag{4}$$

where $G_{H,\min}/2$ is used to avoid overestimation in the coarse height estimation (step 2), in the S-SA estimation. Specifically, if $\Delta T > G_{H,\min}/2$ it may fill the gap with false alarms.

Given assumed time duration of signal and target signal to noise power ratio (SNR), thresholds γ_{step2} and γ_{step3} can be set to minimize RMSE of height estimations in step 2 and step 3.

In FC, there is one design parameter γ_{FC}. This should be more than the false alarm probability of ED since the expected number of false alarms per tile under H_0 is equal to the false alarm probability and it can cancel the false alarms in most cases. In addition, if it is less than the detection probability at ED, it may not degrade the detection performance since the expected number of $D_{n_F,n_T}^{(\mathrm{ED})} = 1$ per tile under H_1 is equal to the detection probability.

5. Numerical Evaluations

In this section, we will evaluate several SA estimation methods (CT-SA, S-SA, and S-SA with FC) and the typical approach, i.e. FT-ED. The evaluated metrics are as follows; receiver operating characteristic (ROC), detection probability, computational time, and amount of required information in terms of spectrum measurement results. Assumptions in the numerical evaluations are as follows. Observed bandwidth is set to 40 MHz, i.e., $f_S = 2B_S = 40$ MHz and the 30-dB bandwidth is set to 22 MHz. This bandwidth is equal to a bandwidth in IEEE 802.11g WLAN since it assumes strong filtering used at the transmitter. Number of samples in a time frame is set to $N_S = 1024$ and the number of samples in segment size of Welch FFT to $N_W = 128$. The number of N_W corresponds to the number of frequency bins. The number of time slots for one observation is set to $N_{\mathrm{timeslot}} = 300$, therefore the time duration of one observation is 7.7 ms. Time duration of one continuous signal (H) and the time gap (G_H) are set to $H = 10$ time slots and $G_H = 8$ time slots, respectively.

To fairly evaluate detection performance, we use CFAR in the evaluations of detection probability, computational time, and the amount of information. The target false alarm rate for output of the SA methods is set to $\tilde{\mathrm{P}}_{\mathrm{FA}}^{(\mathrm{SA})} = 0.01$.

We set Δt and ΔT on the assumption that WLAN is operating in ISM band. Specifically, based on the Monte Carlo simulations we set that $\Delta t = 8$ and $\Delta T = 4$. In addition, $G_{H,\min}$ is set to 8 due to the time duration of DIFS. Moreover, γ_{step2} and γ_{step3} are set based on minimizing RMSE with target SNR being equal to -5 dB, which is reasonable since spectrum measurement and sensing are the most challenging to perform at low SNR values such as -5 dB, i.e. $\gamma_{\mathrm{step2}} = 0.1$ and $\gamma_{\mathrm{step3}} = 0.15$, according to the Monte Carlo simulations. However, analytical derivation of the γ_{step2} and γ_{step3} is one of the future works.

5.1 Detection Performances

In Fig. 8, ROC curves for different methods are plotted. SNR is set to -5 dB. The result reveals that S-SA estimation with FC can achieve the best performance. The S-SA estimation can achieve better performance compared to the CT-SA in the region where $\mathrm{P_{FA}} < 0.1$. On the other hand, in the region where $\mathrm{P_{FA}} \geq 0.1$, they can achieve comparable detection performance. This indicates that the S-SA methods are effective in the low false alarm rate region which is the region of practical interest. For estimation of statistics, such as duty cycle, high false alarm rate may cause bias estimation errors [28].

In Fig. 9, detection rate obtained by Monte Carlo simulation versus SNR is shown. According to the CFAR, false alarm rate for outputs of the SA estimation methods, and the FT-ED are set to 0.01. We can confirm that the S-SA estimation with FC can achieve the best detection performance. Furthermore, detection probability of the S-SA is better than that of CT-SA and the difference in terms of SNR for achieving $P_D = 0.9$ is around 1 dB. The reason why the S-SA can achieve better performance is as follows. ED output $D_{n_F,n_T}^{(\mathrm{ED})}$ for one continuous signal transmission can be divided into several sub-clusters which indicates a cluster in which tiles with $D_{n_F,n_T}^{(\mathrm{ED})} = 1$ are contiguous. The CT-SA can only recognize sub-cluster separately in most of the cases. However, the S-SA can combine several sub-clusters by gap

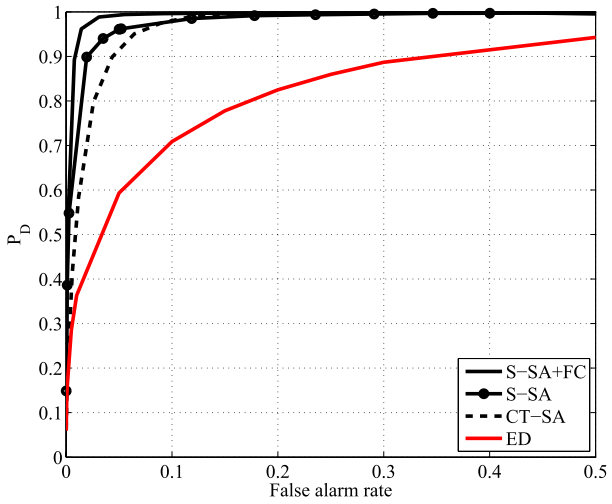

Fig. 8 ROC curves for SA estimation methods and Welch FT-ED. Target SNR is set to −5 dB.

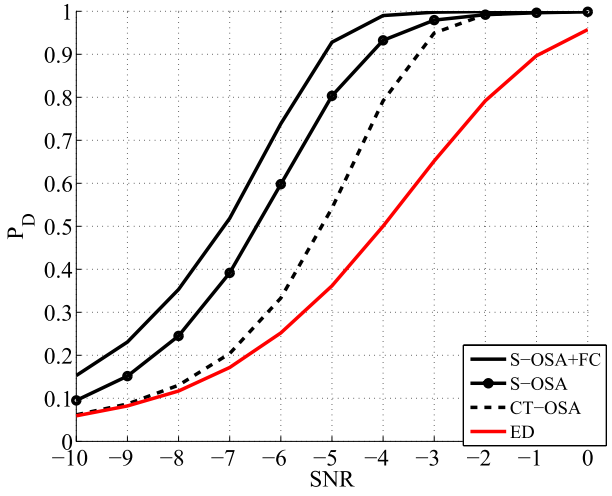

Fig. 9 Detection rate versus SNR.

filling which leads to better detection performance.

Compared to the typical approach, FT-ED, our proposed method S-SA with FC can achieve more than 4 dB gain in SNR for achieving $P_D = 0.9$.

5.2 Computation Time

To evaluate the computational cost, we evaluate computational time for the SA estimation methods in Fig. 10. The algorithms were implemented with MATLAB which was also used to evaluate the computational time of each algorithm. The evaluated computational time represents the time required to perform SA estimation methods for one hundred observations. In the region where SNR is lower than −2 dB, computational times of S-SA based methods (S-SA with FC and S-SA) are faster than that of CT-SA method. This is because S-SA estimates only width (frequency bandwidth) and height (time duration). In addition detection mask based estimation can reduce the computational time compared to

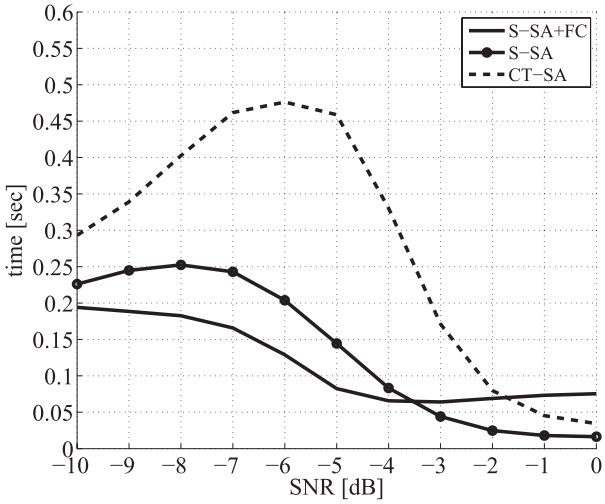

Fig. 10 Computational time as a function of SNR. Computer specifications: Intel Core i7-2600, 3.4 GHz, memory size is 8 GB, and the algorithms were implemented in MATLAB.

the CT-SA which checks the state of each tile one by one.

In the region where SNR is lower than −3.5 dB, S-SA estimation with FC is faster than S-SA estimation. This is a favorable aspect since the region of low SNR values is usually the region of interest in cognitive radio systems. The reason is as follows; once the FC determines that $D^{(\mathrm{ED})}_{n_F,n_T} = 1$ is false alarm component, it will not perform steps 2 and 3 of S-SA estimation as shown in Fig. 7. On the other hand, S-SA estimation performs all of steps.

In the region where SNR is greater than −3.5 dB, the computational time of S-SA estimation with FC slightly increases and the time of S-SA estimation with FC is more than that of S-SA estimation. The increment of the computational time is related to required false alarm rate at ED (Input $\mathrm{P_{FA}}$) in S-SA estimation with FC. Specifically, the false alarm rate of the ED is set to satisfy the target false alarm rate at output of S-SA estimation with FC, i.e. $\tilde{\mathrm{P}}_{\mathrm{FA}}^{(\mathrm{S-SA-FC})} = 0.01$. Fig. 11 shows required $\mathrm{P_{FA}}^{(\mathrm{ED})}$ for SA estimation methods to satisfy the target false alarm rate as $\tilde{\mathrm{P}}_{\mathrm{FA}}^{(\mathrm{SA})} = 0.01$. In the region where SNR is greater than −5 dB, P_{FA} at ED for S-SA with FC increases. This implies that the FC can cancel more false alarm components when SNR increases. In other words, $\mathrm{P_{FA}}^{(\mathrm{ED})}$ increases to satisfy the target P_{FA}, which is beneficial since this means also increased detection probability per tile. The increment of computational time in S-SA estimation with FC is caused by the process of FC for canceling increased false alarms.

We have also evaluated the computational time when the PU is inactive under the same situation as Fig. 10. The results are as follows: S-SA with FC: 0.95 sec, S-SA: 0.13 sec, and CT-SA: 0.15 sec. We can confirm that S-SA with FC and S-SA can achieve better performance compared to CT-SA.

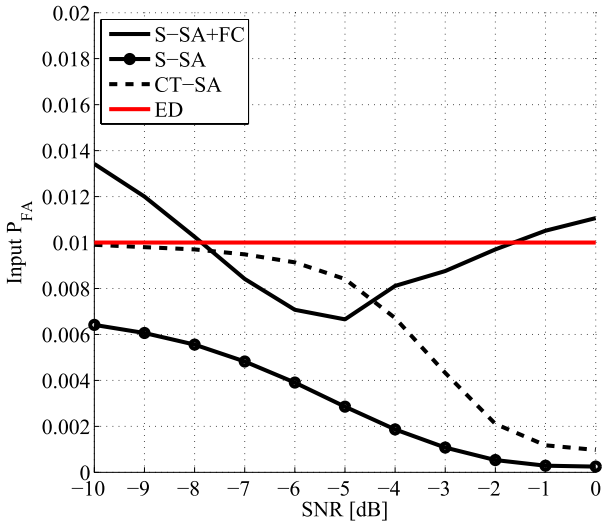

Fig. 11 Input P_{FA} to satisfy target false alarm rate 0.01 as a function of SNR. In the case of ED, there is no preprocessing, therefore input P_{FA} is equal to the target $P_{FA} = 0.01$.

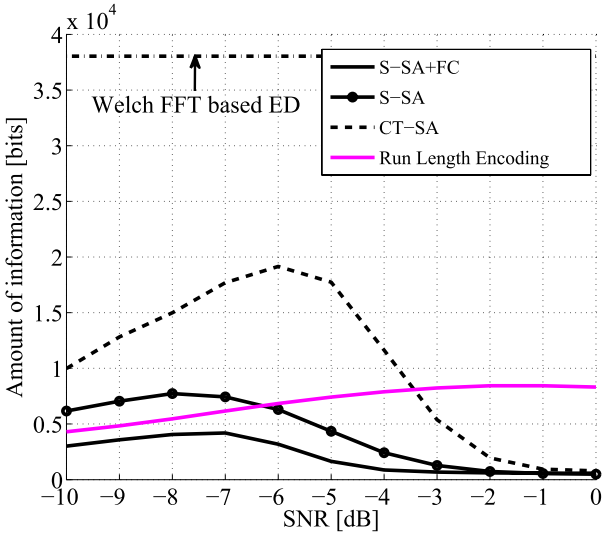

Fig. 12 Amount of information as a function of SNR.

5.3 Amount of Information

In Fig. 12, the amount of information for one observation as a function of SNR is shown. In case of the FT-ED, the amount of observed information corresponds to the number of tiles in the observed space, Therefore the amount of information for one observation is 3.8×10^4 bits as shown in Fig. 12.

In the SA methods, amount of information is proportional to the number of estimated rectangles. In the low SNR region, such as when SNR is lower than −8 dB for S-SA with FC, the amount of information increases when SNR increases. The increased amount of information in the low SNR region is caused by the increased detection probability. In the low SNR region, it is difficult to detect one actual SA provided by one data packet correctly and it may be divided into several estimated rectangle SAs.

On the other hand, in the high SNR region such as when SNR is greater than −7 dB for S-SA with FC, the amount of information decreases. The reason of this decrease is also due to the increase of detection probability. Specifically, S-SA begins to detect the actual SA correctly and the number of divides in terms of one actual SA decreases with increased SNR. In addition, at the SNR where $P_D{}^{(\cdot)} \approx 1$ the amount of information is saturated since it can detect the actual SAs correctly.

On the other hand, in the case of SA methods, coordinates are utilized. Amount of information for actual SA is about $(\lceil \log_2(300) \rceil + \log_2(128)) + (\lceil \log_2(60) \rceil + \lceil \log_2(10) \rceil) = 26$ bits, where 60 is the number of bins for signal occupancy (22 MHz). For one observation (300 time slots), there are $300/18 \approx 16.6$ actual SAs. Then, the amount of information for one observation is equal to $26 \times 16.6 \approx 433$ bits which is the saturated value.

In a practical situation, we need to predetermine the numbers of bits for height and width estimations, respectively. It is possible to update the numbers in each frame by using the maximum values of the estimations. In the evaluations in Fig. 12, it is equivalent to determining the numbers of bits optimally in each time frame.

We also evaluate run length encoding (RLE) [29] for the output of FT-ED. Again in the low SNR (lower than −4 dB), amount of information for RLE increases with the increase in SNR. The main reason of this aspect is that in the low SNR the amount of information is slightly lower due to low detection probability. At SNR = −2 dB, the amount of information for RLE is saturated and the saturated value is still larger than that of the SA approaches.

6. Conclusion

In this paper, we have investigated SA estimation techniques for spectrum measurement. To perform proper measurement, the OE is required to be able to achieve adequate detection accuracy at relatively low computational cost as well as low amount of information in terms of local observations. A typical approach for spectrum measurement is FT-ED, however it cannot achieve adequate detection accuracy. For this issue, we have proposed a simple SA estimation method, S-SA. The S-SA is designed to estimate rectangular SA efficiently. Specifically, the S-SA only estimates the location and the width and height and it leads to less complexity. In addition, diversity gain is available due to the covering several tiles. Therefore SA can improve detection probability however, it inherently increases false alarm rate. Therefore, we have proposed FC technique for this issue. Numerical results showed that the proposed method, S-SA with FC, can achieve the best detection performance. In addition, it is also possible to achieve short computational time especially in the low SNR region. Furthermore, the amount of information of spectrum observation can be reduced by considering the rectangular shape of the SA.

Acknowledgment

This research was supported by the Strategic Information and Communications R&D Promotion Programme (SCOPE). The work of Janne J. Lehtomäki was supported by SeCoFu project of the Academy of Finland.

References

[1] I.F. Akyildiz, W.-Y. Lee, M.C. Vuran, and S. Mohanty, "A survey on spectrum management in cognitive radio networks," IEEE Commun. Mag., vol.46, no.4, pp.40–48, April 2008.
[2] J. Mitola and G.Q. Maguire, "Cognitive radio: Making software radios more personal," IEEE Pers. Commun., vol.6, no.4, pp.13–18, Aug. 1999.
[3] Q. Zhao and B.M. Sadler, "A survey of dynamic spectrum access," IEEE Signal Process. Mag., vol.24, no.3, pp.79–89, May 2007.
[4] I.F. Akyildiz, W.-Y. Lee, M.C. Vuran, and S. Mohanty, "NeXt generation/dynamic spectrum access/cognitive radio wireless networks: A survey," Computer Networks, vol.50, no.13, pp.2127–2159, Sept. 2006.
[5] T. Yucek and H. Arslan, "A survey of spectrum sensing algorithms for cognitive radio applications," IEEE Commun. Surv. Tutorials, vol.11, no.1, pp.116–130, 2009.
[6] M. Fitch, M. Nekovee, S. Kawade, K. Briggs, and R. MacKenzie, "Wireless service provision in TV white space with cognitive radio technology: A telecom operator's perspective and experience," IEEE Commun. Mag., vol.49, no.3, pp.64–73, 2011.
[7] K. Umebayashi, S. Tiiro, and J.J. Lehtomäki, "Development of a measurement system for spectrum awareness," Proc. 1st International Conference on 5G for Ubiquitous Connectivity, pp.234–239, 2014.
[8] N. Wang, Y. Gao, and X. Zhang, "Adaptive spectrum sensing algorithm under different primary user utilizations," IEEE Commun. Lett., vol.17, no.9, pp.1838–1841, Sept. 2013.
[9] T. Nguyen, B.L. Mark, and Y. Ephraim, "Spectrum sensing using a hidden bivariate Markov model," IEEE Trans. Wireless Commun., vol.12, no.9, pp.4582–4591, Sept. 2013.
[10] D. Zhao and X. Zhou, "Spectrum sensing using prior probability prediction," Proc. 2011 7th International Conference on Wireless Communications, Networking and Mobile Computing, pp.1–4, 2011.
[11] J. Vartiainen, M. Höyhtyä, J. Lehtomäki, and T. Bräysy, "Priority channel selection based on detection history database," Proc. 5th International ICST Conference on Cognitive Radio Oriented Wireless Networks and Communications, pp.1–5, 2010.
[12] K. Umebayashi, Y. Suzuki, and J.J. Lehtomäki, "Dynamic selection of CWmin in cognitive radio networks for protecting IEEE 802.11 primary users," Proc. 6th International ICST Conference on Cognitive Radio Oriented Wireless Networks and Communications, pp.266–270, 2011.
[13] Y. Xu, A. Anpalagan, Q. Wu, L. Shen, Z. Gao, and J. Wang, "Decision-theoretic distributed channel selection for opportunistic spectrum access: Strategies, challenges and solutions," IEEE Commun. Surv. Tutorials, vol.15, no.4, pp.1689–1713, 2013.
[14] T.M. Taher, R.B. Bacchus, K.J. Zdunek, and D.A. Roberson, "Long-term spectral occupancy findings in Chicago," 2011 IEEE International Symposium on Dynamic Spectrum Access Networks (DySPAN), pp.100–107, 2011.
[15] M. Mehdawi, N. Riley, K. Paulson, A. Fanan, and M. Ammar, "Spectrum occupancy survey in HULL-UK for cognitive radio applications: Measurement & analysis," International Journal of Scientific & Technology Research, vol.2, no.4, pp.231–236, April 2013.
[16] M. López-benítez and F. Casadevall, "Spectrum usage in cognitive radio networks: From field measurements to empirical models," IEICE Trans. Commun., vol.E97-B, no.2, pp.242–250, Feb. 2014.
[17] H. Urkowitz, "Energy detection of unknown deterministic signals," Proc. IEEE, vol.55, no.4, pp.523–531, 1967.
[18] J. Vartiainen, J. Lehtomäki, T. Bräysy, and K. Umebayashi, "Spectrum sensing in public safety applications: The 2-D LAD ACC method," Proc. 6th International ICST Conference on Cognitive Radio Oriented Wireless Networks and Communications, pp.61–65, 2011.
[19] J. Vartiainen, H. Sarvanko, J. Lehtomaki, M. Juntti, and M. Latva-aho, "Spectrum sensing with LAD-based methods," Proc. 2007 IEEE 18th International Symposium on Personal, Indoor and Mobile Radio Communications, pp.1–5, 2007.
[20] M. López-Benítez and F. Casadevall, "Improved energy detection spectrum sensing for cognitive radio," IET Commun., vol.6, no.8, pp.785–796, May 2012.
[21] J. Kokkoniemi and J. Lehtomaeki, "Spectrum occupancy measurements and analysis methods on the 2.45 GHz ISM band," Proc. 7th International Conference on Cognitive Radio Oriented Wireless Networks, pp.285–290, 2012.
[22] D.W. Capson, "Performance comparisons of contour extraction algorithms," IEEE Trans. Instrum. Meas., vol.IM-35, no.4, pp.409–417, Dec. 1986.
[23] P.D. Welch, "The use of fast Fourier transform for the estimation of power spectra: A method based on time averaging over short, modified periodograms," IEEE Trans. Audio Electroacoust., vol.15, no.2, pp.70–73, June 1967.
[24] K. Umebayashi, R. Takagi, N. Ioroi, Y. Suzuki, and J.J. Lehtomäki, "Duty cycle and noise floor estimation with Welch FFT for spectrum usage measurements," Proc. 9th International Conference on Cognitive Radio Oriented Wireless Networks, pp.73–78, 2014.
[25] "Recommendation ITU-R SM.328-10. Spectra and bandwidth of emissions," 1992.
[26] J. Serra, Image Analysis and Mathematical Morphology, Academic Press, 1983.
[27] J.J. Lehtomaki, R. Vuohtoniemi, and K. Umebayashi, "On the measurement of duty cycle and channel occupancy rate," IEEE J. Sel. Areas. Commun., vol.31, no.11, pp.2555–2565, Nov. 2013.
[28] H. Iwata, K. Umebayashi, S. Tiiro, Y. Suzuki, and J.J. Lehtomaki, "Optimum welch FFT segment size for duty cycle estimation in spectrum awareness system," 2015 IEEE Wireless Communications and Networking Conference Workshops (WCNCW), pp.229–234, 2015.
[29] J. Capon, "A probabilistic model for run-length coding of pictures," IEEE Trans. Inf. Theory, vol.5, no.4, pp.157–163, Dec. 1959.

Kenta Umebayashi received LL.B., degree from Ritsumeikan University in 1996, B.E., M.E., and Ph.D. degrees from the Yokohama National University in 1999, 2001, and 2004, respectively. From 2004 to 2006, he was a research scientist at the University of Oulu, Centre for Wireless Communications (CWC). He is currently an associate professor in the Tokyo University of Agriculture and Technology. In 2010, he was a visiting professor at the University of Oulu. His research interests lie in the areas of signal detection theory and wireless communication systems, cognitive radio. He received the Best Paper Award in IEEE WCNC 2012 for a paper he authored.

Kazuki Moriwaki received B.E. and M.E. degrees from Tokyo University of Agriculture and Technology, Tokyo, Japan, in 2013 and 2015. His research interests are cognitive radio and wireless communication systems.

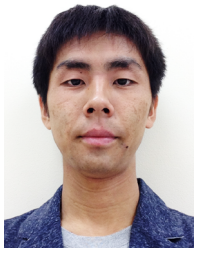

Riki Mizuchi received B.E. degree from Tokyo University of Agriculture and Technology, Tokyo, Japan, in 2015. His research interests are cognitive radio and wireless communication systems.

Hiroki Iwata received B.E. degree from Tokyo University of Agriculture and Technology, Tokyo, Japan, in 2014. His research interests are cognitive radio networks, spectrum measurement and wireless communication systems.

Samuli Tiiro received the M.Sc. degree in information engineering from University of Oulu in 2008, and the Ph.D. degree in electronic and information engineering from Tokyo University of Agriculture and Technology in 2014. Currently, he is a postdoctoral research fellow in Tokyo University of Agriculture and Technology. His research interests include cognitive radio and dynamic spectrum access techniques, focusing on measurement and prediction of spectrum utilization.

Janne J. Lehtomäki got his doctorate in wireless communications from the University of Oulu in 2005. Currently, he is a senior research fellow at the University of Oulu, Centre for Wireless Communications. He spent the fall 2013 semester at the Georgia Institute of Technology, Atlanta, USA, as a visiting scholar. Currently, he is focusing on communication techniques for networks composed of nanoscale devices. Dr. Lehtomaki has served as a guest associate editor for the IEICE Transactions on Communications Special Section (Feb. 2014) and as a managing guest editor for Nano Communication Networks (Elsevier) Special Issue (Dec. 2015). He co-authored the paper receiving the Best Paper Award in IEEE WCNC 2012. He is editorial board member of Physical Communication (Elsevier) and was the TPC co-chair for IWSS Workshop at IEEE WCNC 2015 and publicity chair for ACM NANOCOM 2015. Dr. Lehtomaki has published more than 100 papers in journals and conferences.

Miguel López-Benítez received the B.Sc. (2003) and M.Sc. (2006) degrees in Communications Engineering (First-Class Distinctions) from Miguel Hernández University (UMH), Elche, Spain, and the Ph.D. degree (2011) in Communications Engineering (2011 Outstanding Ph.D. Thesis Award) from the Department of Signal Theory and Communications of the Technical University of Catalonia (UPC), Barcelona, Spain. From 2011 to 2013 he was a Research Fellow in the Centre for Communication Systems Research of the University of Surrey, Guildford, United Kingdom. Since 2013 he has been a Lecturer (Assistant Professor) in the Department of Electrical Engineering and Electronics of the University of Liverpool, United Kingdom. His research interests are in the field of wireless communications and networking, with special emphasis on cellular mobile communications and dynamic spectrum access in cognitive radio systems. He was the recipient of the IEICE-CS Best Tutorial Paper Award 2014, among others (see http://www.lopezbenitez.es for details).

Yasuo Suzuki was born in Tokyo, Japan, in August, 1950. He received the B.E. degree from Saitama University, Urawa, Japan, in 1973 and the D.E. degree from Tokyo Institute of Technology, Tokyo, Japan, in 1985. In 1973, he joined Toshiba Corporation, where he worked on the development of various antenna including adaptive antenna for radar, communications, and navigations. In April 2000, he moved from Toshiba Corporation to Tokyo University of Agriculture and Technology, where he is now a professor of the Department of Electrical and Electronic Engineering. His current research interests include the applications of wireless and antenna technologies to mobile communications. He has experienced a wide range of research and development work, such as for array antennas, adaptive antennas, aperture antennas, micro-strip antennas, ultra-compact radio equipment, software defined radio, and so on. He is the coauthor of seven books. He received Paper Award from the IEICE 2002. Prof. Suzuki is an IEICE fellow.